

Supporting Information

Early bacteriopheophytin reduction in charge separation in reaction centers of *Rhodobacter sphaeroides*

Jingyi Zhu^{*}, Ivo H. M. van Stokkum^{*}, Laura Paparelli^{*}, Michael R. Jones[†], Marie Louise Groot^{*‡}

^{*} Department of Physics, Faculty of Sciences, VU University Amsterdam, De Boelelaan 1081, 1081 HV Amsterdam, The Netherlands

[†] School of Biochemistry, Medical Sciences Building, University of Bristol, University Walk, Bristol, BS8 1TD, United Kingdom

[‡] corresponding author, email m.l.groot@vu.nl

Correction for baseline fluctuations in the near-IR data.

The matrix of the residuals of the near-IR data is highly structured due to baseline fluctuations. This structure is revealed by a singular value decomposition of the matrix of the residuals (48). The screenplot with the logarithm of the singular values, Figure S1E indicates that the first singular value of the matrix of the residuals stands out, and is responsible for a large part of the rms error of the fit. The first right singular vector (Figure S1D) consists of a constant term plus a wiggle, and represents the baseline fluctuations, noise that is highly correlated in the time gated spectra. The first left singular vector (Figure S1C) is unstructured, indicating that there is no correlation in the noise between subsequent spectra. We therefore subtracted these estimated baseline fluctuations from the data, thereby reducing the rms error of the fit from 0.450 mOD to 0.203 mOD. Representative traces at 960 and 1025 nm before and after the correction for baseline fluctuations are depicted in Figure S1A,B (before) and Figure S1F,G (after).

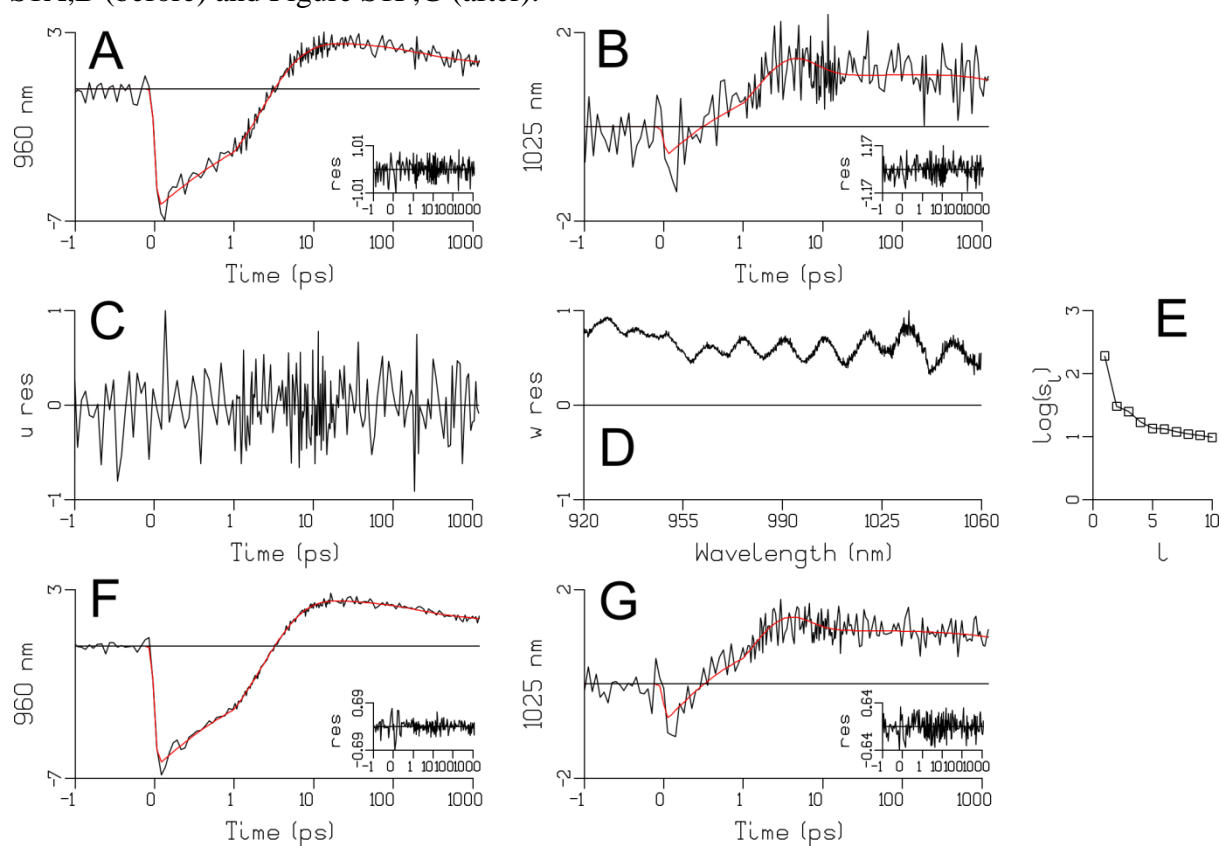


Figure S1. Representative traces at 960 and 1025 nm before (A,B) and after (F,G) the correction for baseline fluctuations. Red lines indicate global fits using four lifetimes. Note that the time axis is linear until 1 ps, and logarithmic thereafter. Insets show residuals. Results from Singular Value Decomposition of the matrix of the residuals: first left (C) and right (D) singular vector, and screeplot with the logarithm of the singular values.

Distributed fit of the near IR data

A global fit using four monoexponential decays results in the four decay associated difference spectra (DADS) of Figure S2B. The two fastest estimated lifetimes are 1.5 and 3.4 ps. The third lifetime was fixed at 200 ps, in view of the visible region data where this value was estimated. The fourth lifetime was much larger than the 1 ns measurement window. The fourth DADS (light green) can be interpreted as P^+ , the third DADS can be interpreted as H_A^- . The second DADS (red) can be interpreted as decay of P^* (stimulated emission above 920 nm) in combination with rise of the B_A^- band around 1025 nm. Because of the inverted kinetics this rise is a positive feature in the red DADS, and a negative feature in the black DADS (1). The broad negative feature in the black DADS below 990 nm is more difficult to assign. In combination with the 920-955 nm positive feature superimposed on the red 3.4 ps DADS it represents early $P^+H_A^-$.

When the fastest two decays are assumed to be normally distributed (2) on a logarithmic scale, $\int_{-\infty}^{\infty} \exp(-(\log(k) - \log(k_c))^2 / (2\sigma^2)) \{ \exp(-kt) \otimes IRF(t) \} d \log(k)$, the distributions depicted in Figure S2E are estimated. The shapes of the red, blue and green DADS in Figure S2D and B are identical, but the black DADS is different below 990 nm, due to the “faster decay part” of the second component. The rms error of the fit is only slightly better (0.1%), indicating that the data are consistent with the fast decays being monoexponential or distributed. For target analysis the distributions of the two fast decays can be mimicked by a heterogeneous model with a linear combination of exponentials for the formation of the $P^+B_A^-$ and $P^+H_A^-$ states. From the overlap of the black and red distributions we infer that there are two extremes for the formation of the $P^+B_A^-$ and $P^+H_A^-$ states: fast – fast, resulting in early $P^+H_A^-$, and slow – slow resulting in the ≈ 3.4 ps P^* decay and an appreciable transient population of $P^+B_A^-$.

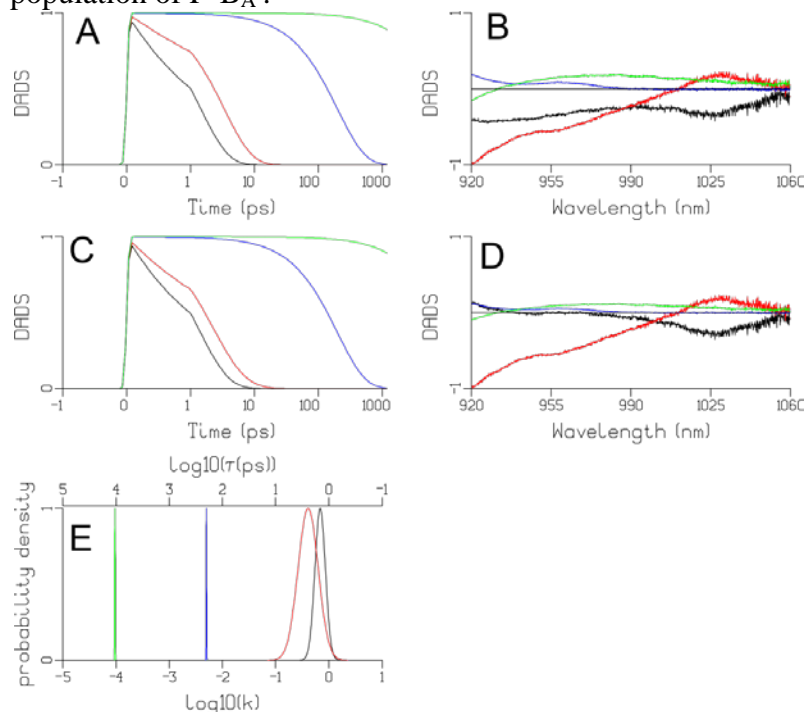


Figure S2. Global analysis of the near IR data using four monoexponential decays (A,B) or two distributed decays and two monoexponential decays (C,D,E). Key: black 1.5 ps (A) and $k_c=0.7/\text{ps}$ (C), red 3.4 ps and $k_c=0.4/\text{ps}$ (C), blue 200 ps, green long lived. Time axis in (A,C) is linear until 1 ps, and logarithmic thereafter.

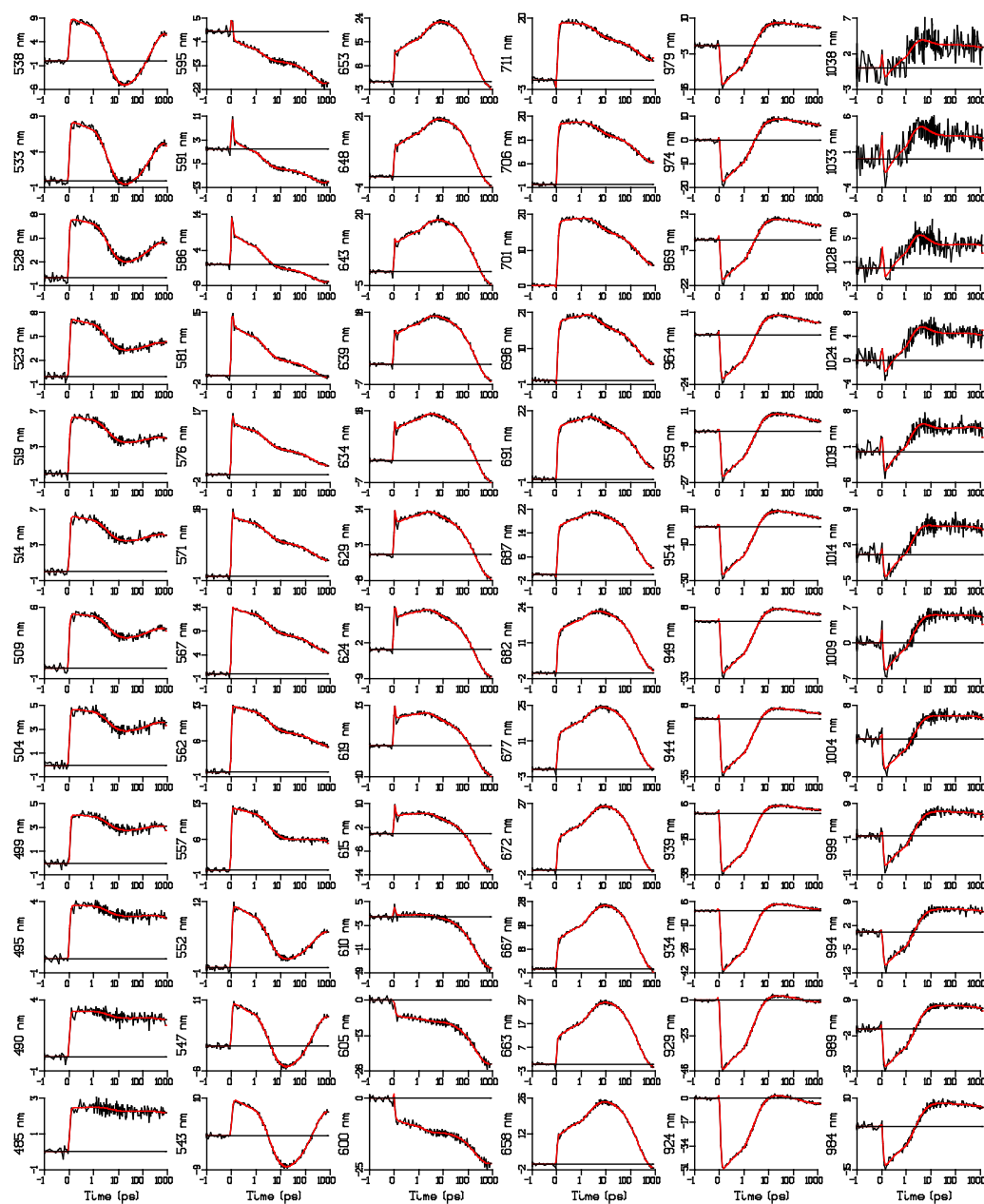


Figure S3. Time decay traces after excitation of P at representative wavelengths (ordinate labels) of data (black) and fit (red) according to the heterogeneous kinetics model as in Figure 4. Time axis is linear until 1 ps, and logarithmic thereafter. Spikes straddling time zero are attributed to coherent artifact.

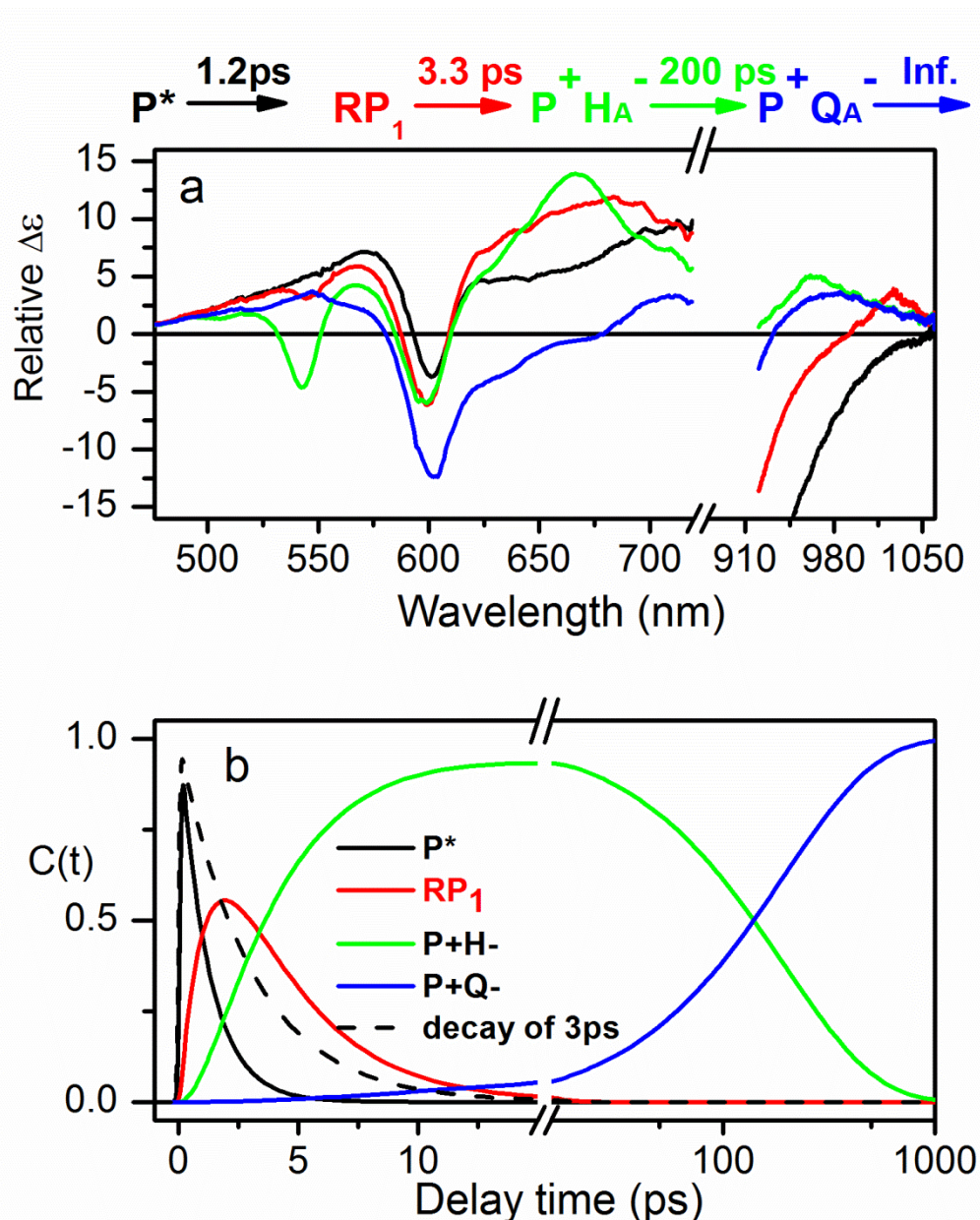


Figure S 4. Result of global fitting based on a sequential scheme with increasing lifetimes. (A) Model, fitted SADS and time constants. (B) Fitted populations of each state according to the model in (A). Although this model yielded a better separation of the species RP_1 and $P^+H_A^-$ in the NIR region there were three reasons to discard it: 1) a clear contribution from P^* emission was still present at 960 nm in this SADS of the RP_1 state; 2) the lifetime of P^* was too short to match the observed P^* fluorescence life time of ≈ 3 ps (represented by the dashed line in panel B); 3) the intensities of the bleach at around 600 nm for RP_1 and $P^+H_A^-$ were not consistent with expectations. Kirmaier et al (3) have shown that the bleach at 600 nm for $P^+B_A^-$ is larger than for $P^+H_A^-$ by comparing the spectroscopic differences between wild-type RCs and a L214H mutant in which the H_A BPheo is replaced by a BChl.

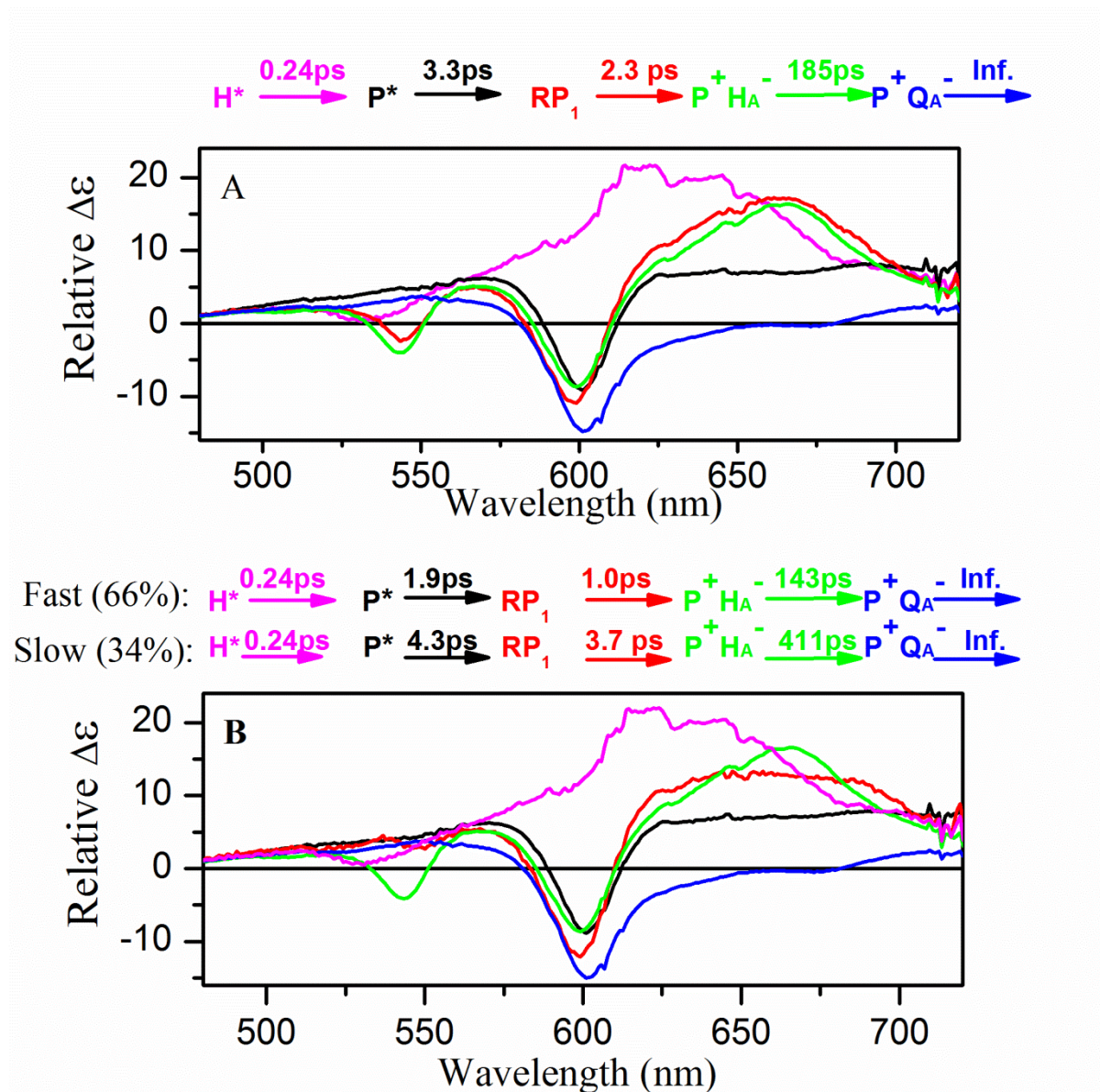


Figure S 5. Target analysis of absorbance difference spectra after excitation of H. (A) Reaction model with inverted kinetics (top) and SADS obtained from fitting this model to the experimental data. The SADS are colour coded with the reaction model. (B) Reaction model with heterogeneous fast and slow populations, both exhibiting inverted kinetics and estimated SADS.

SUPPORTING REFERENCES

1. Van Stokkum, I. H. M., Beekman, L. M. P., Jones, M. R., van Brederode, M. E., and van Grondelle, R. 1997. Primary electron transfer kinetics in membrane-bound *Rhodobacter sphaeroides* reaction centers: A global and target analysis. *Biochemistry* 36, 11360-11368.
2. Beekman, L. M. P., vanStokkum, I. H. M., Monshouwer, R., Rijnders, A. J., McGlynn, P., Visschers, R. W., Jones, M. R., and vanGrondelle, R. 1996. Primary electron transfer in membrane-bound reaction centers with mutations at the M210 position. *Journal of Physical Chemistry* 100, 7256-7268.
3. Kirmaier, C., Gaul, D., Debey, R., Holten, D., and Schenck, C. C. 1991. Charge Separation in a Reaction Center Incorporating Bacteriochlorophyll for Photoactive Bacteriopheophytin. *Science* 251, 922-927.